IR MATERIAL RESEARCH AT THE ARMY RESEARCH LABORATORY

Herbert Pollehn, KK Choi, Stefan Svensson, Nibir Dhar
US Army Research Laboratory 2800 Powder Mill Rd, Adelphi MD 20783

ABSTRACT

Research on Mercury Cadmium Telluride (HgCdTe or MCT) and group III-V based infrared materials is being conducted for the development of advanced, especially large area IR detector and focal plane arrays. The focus of this research has been on materials for Quantum Well Infrared Photo Detectors (QWIPs), Sb based type II superlattice detectors, Silicon based substrates for MCT detectors and MCT detectors with higher operating temperature. Recently research has been initiated in dilute Nitride materials.
To improve the quantum efficiency, reproducibility and operating temperature of the QWIP detectors, a corrugated design has been implemented. For superlattice detectors, focal plane arrays for the MWIR spectral band have been successfully demonstrated and good image quality has been obtained. Current efforts are concentrated on achieving high quality materials and passivation techniques for the LWIR spectral band. A recently initiated effort on dilute Nitride materials holds the premise to obtain high quality direct bandgap detectors with III-V materials. For MCT detectors on Si based substrates MWIR detectors have been demonstrated with high quality, but for LWIR detector arrays of sufficient low defect densities have not been obtained on a consistent basis. Recent efforts showing promising results will be discussed.

INTRODUCTION

US military rules of engagement require identification of targets before engagement. Persistent surveillance of large areas has also become an urgent need for military operations. Translating these applications into imaging system requirements calls for very high resolution (up to 4000X4000 pixels), high sensitivity and dual/multi color operation. Other very important factors are cost and reliability. For these reasons a new class of IR focal plane arrays have to be developed featuring very large staring formats but at the same time keeping down production cost and being highly reliable.
The US Army Research Laboratory is engaged in a research program to lay the foundation for fulfilling these requirements. In this research program three different approaches are taken ;
1) Improve QWIPs in respect to it's quantum efficiency, operating temperature and reproducibility. Broad band and multi color operation are also desirable characteristics.
2)Develop type II superlattice structures for IR detectors . These types of detectors hold great promise for high operating temperature, high quantum efficiency and relative low production cost.
The assumption of relative low production cost for both the QWIP and the superlattice detector is based on their III-V materials characteristics. III-V materials are used for a number of other devices and substrates for their growth are readily available in large sizes. .
3)Develop the technology to grow HgCdTe on Silicon substrates for both MWIR and LWIR focal plane arrays. HgCdTe detectors have clearly demonstrated the required high

Infrared Technology and Applications XXXIII, edited by Bjørn F. Andresen, Gabor F. Fulop, Paul R. Norton,
Proc. of SPIE Vol. 6542, 65420C, (2007) · 0277-786X/07/$18 · doi: 10.1117/12.723659

quantum efficiency, but for large area staring arrays, the cost for the standard CdZnTe substrate will be very high and reliability is questionable.
Dual color operation has been demonstrated for QWIPs and HgCdTe focal plane arrays and should be of no more difficulty for the superlattice detectors once this material system has been fully developed. Technologies to obtain dual color operation will not be discussed in this paper.

CORRUGATED QUNATUM WELL INFRARED PHOTODETECTORS

Background

Quantum well infrared photodetectors (QWIPs) are based on the well established GaAs material technology. The detectors are therefore potentially manufacturable in large quantities and at low cost. For example, a single material growth run in a Riber 7000 MBE reactor can yield fourteen 4" wafers or seven 6" wafers, and each 4" wafer yields 11 FPAs in 1024 × 768 HDTV format. A wafer growth run can therefore yield up to 154 FPAs. Combining with the widely available low cost substrates, the material cost per die is rather small.
Furthermore, the predictability of the material quality eliminates most of the cost related to material development, characterization and repeated growth runs. Therefore, the substantial cost for an FPA, other than that related to readout circuits, reduces to its fabrication cost. In the standard QWIP FPA production, most of the processes such as mesa delineation and metal contact deposition are routine processes. The more challenging step is in the grating fabrication. In this process, a series of test structures with different grating periods and depths are fabricated on a sample wafer and characterized to determine its proper parameters. Assuming other wafers being identical, the same grating structure can be adopted in production. Obviously, this process is labor intensive and time consuming, and it may require new masks and fabrication procedures for the new grating structures. Even with this pilot procedure, desirable performance may not be ensured if the wafers were not identical. In addition, because of the fine features in the gratings, slow processes such as step and repeat printing and e-beam lithography may be needed in some wavelength regimes. After readout hybridization, complete substrate removal is mandated to eliminate pixel cross-talk due to grating diffraction. At ARL, we collaborated with L3-Cincinnati Electronics and NASA Goddard Space Center to produce QWIP FPAs based on a wavelength independent detector geometry, which is known as the corrugated-QWIP (or C-QWIP). This detector geometry relies on angled sidewalls to reflect light for absorption and thus eliminates the need for gratings. Under this coupling scheme, the same detector geometry is efficient for all wavelengths and it does not contain fine features. The same masks and fabrication procedures are therefore suitable for any wafer materials. No prior knowledge on the wafers is needed. The FPAs can therefore be fabricated by standard and high throughput batch processes. Together with the resulting high yield, which at present is about 70%, the C-QWIP detector thus paves the way for low cost, large format and high sensitivity FPA production.

Detection wavelength of QWIPs

To assess the variation of the wafer materials in production, we calculated the absorption spectrum of an $Al_xGa_{1-x}As/In_yGa_{1-y}As$ multiple quantum well structure. Each well contains 7Å GaAs/ 35A InGaAs/ 7Å GaAs. To obtain the peak absorption wavelength, λ_p, we calculated the eigen energies and eigen functions of the structure, and obtained the oscillator strength for each transition [1]. Fig. 1(a) shows the calculated λ_p as a function of x and y. From Fig. 1(a), if the MBE composition varies by 2% within the growth

chamber, the absorption wavelength can vary by 1 μm in the vicinity of 8.3 μm peak. We further adjusted the linewidth of the individual transitions to fit the experimental lineshape, and obtained the corresponding cutoff wavelengths λ_c shown in Fig. 1(b). It again shows that a 2% variation of material composition can change the cutoff by 1 μm. Since this level of wavelength variation is observed among different wafers within the same growth run or among different growth runs, the exact λ_p of individual wafers cannot be ascertained by a sample wafer. A wavelength independent coupling structure is thus much needed for volume production. Figure 2 shows the spectral responsivity of two wafers grown at the same time. Both λ_p and λ_c differ by approximately 1.0 μm, which indicates the compositional nonuniformity to be about 2%.

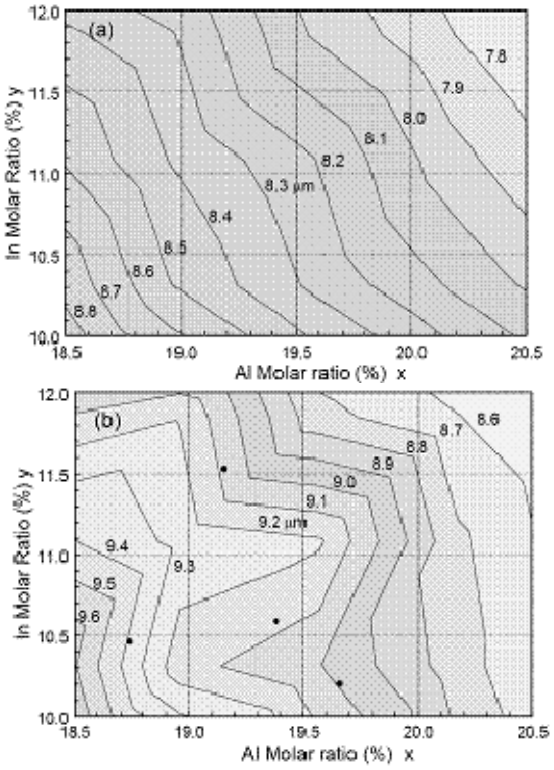

Fig. 1. The calculated peak absorption wavelength (a) and the cutoff wavelength (b) for different values of x and y in an $Al_xGa_{1-x}As/In_yGa_{1-y}As$ multiple quantum well structure. The black circles show the compositions of the experimental detectors from which the theoretical cutoff fitting is based on.

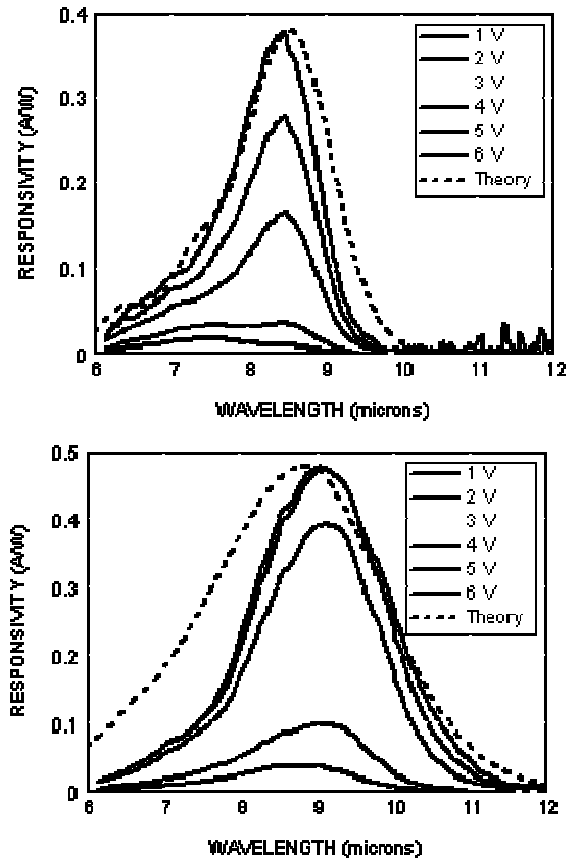

Fig 2. The spectral responsivity of two different wafers grown in the same run. The material structure obtained from a sample piece is: x = 0.1874, y = 0.1046 and w = 7Å/35Å/7Å. The dash curves are theoretical calculations. To fit the experimental spectra with the indicated composition, the GaAs/AlGaAs band offset has to be set at $0.732\Delta E_g$ for (a) and $0.67\Delta E_g$ for (b) because of the different spectrum.

C-QWIP FPAs

The C-QWIP pixel geometry is shown in Fig. 3. A C-QWIP contains an MgF_2/Au cover layer for sidewall protection [2]. This cover layer is electrically isolated from the top and bottom contacts of the pixels as shown in Fig. 3. Fig. 4 shows the fabricated 1024 × 1024 FPAs and the 1024 × 768 FPAs on 4" wafers. Readout hybridization was performed at L3-Cincinnati Electronics.

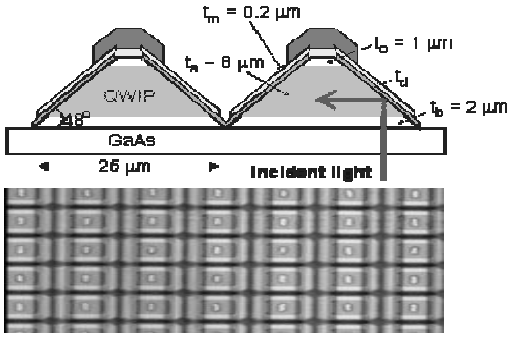

Fig. 3. The side view of the C-QWIP pixels with 25 μm pitch (left) and the top view of the pixels (below).

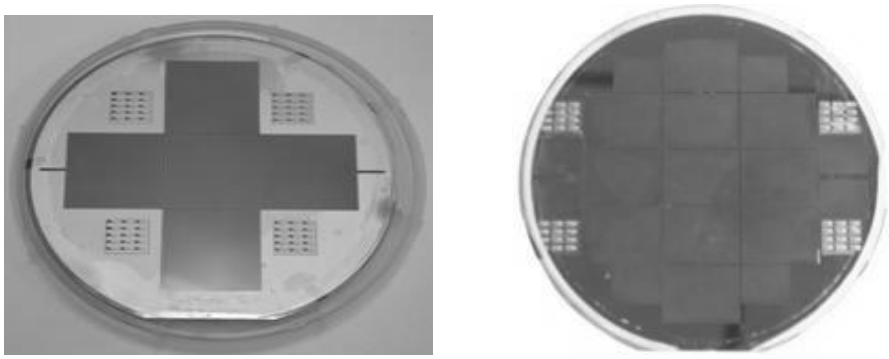

Fig. 4. The top views of five 1024 × 1024 C-QWIP FPAs (left) and eleven 1024 × 768 C-QWIP FPAs (right) on 4" wafers (right). There are also spare rooms for smaller format FPAs if desired.

C-QWIP FPA Performance

Figures 5, 6 and 7 show the spectral responses and images of three 1024 × 1024 C-QWIP FPAs with cutoff at 8.3, 9.0 and 11.6 μm, respectively. All three FPAs have exactly the same detector geometry as depicted in Fig. 3.

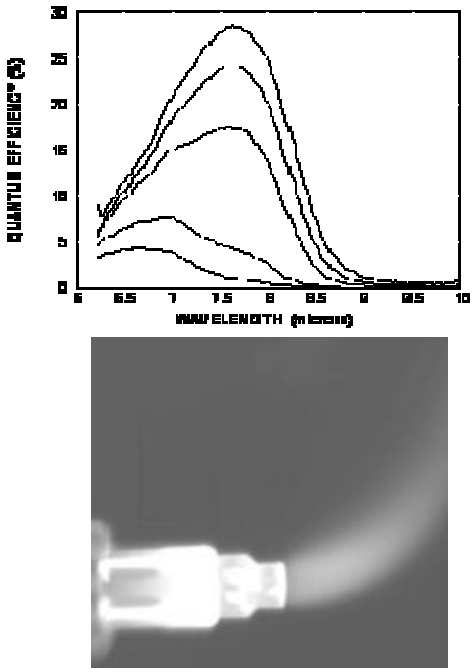

Fig. 5. The predicted QE of a 8.3 μm C-QWIP pixel (left) at 3, 5, 7, 9, 11 and 13 V, respectively. The measured FPA QE at 13 V is 35%. The image of a torch flame taken at L3-CE is on the right.

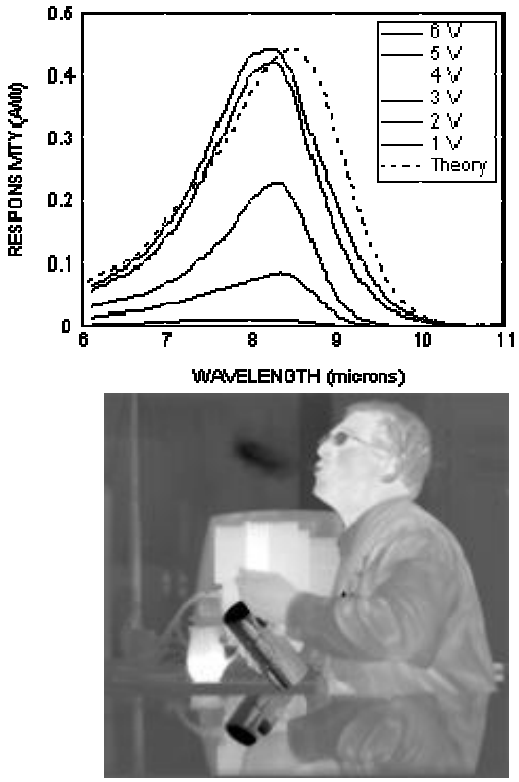

Fig. 6. The responsivity of a 9.0 μm edge coupled QWIP (left), and the image taken by the corresponding C-QWIP FPA at L3-CE (right). The QE of a fan-out pixel was determined to be 33% at 6V and 77K.

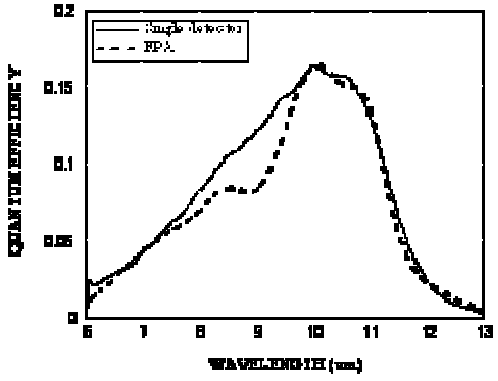

Fig. 7. The measured QE of the C-QWIP FPA (dashed curve) and the spectral shape of an edge coupled detector (red curve) at 3V (left). The QE of the FPA is 26.3% at 5V based on single detector characteristics. The image taken by the FPA at NASA GSFC is on the right.

Conclusion

In this section, we have pointed out, that due to the inevitable wavelength variations among different wafer materials, there is a need for a wavelength independent detector geometry in volume production. By adopting the C-QWIP geometry, the natural absorption wavelength of individual wafers can be preserved without prior knowledge of the wafers. In the present FPAs, a QE of 20 – 35% is achievable with certain detector parameters and under certain operating conditions. Further improvement is expected with more optimized structures such as pixels with all angled sidewalls or completely removed substrates. Combining high efficiency with its simplistic processing steps, the C-QWIP structures are thus ideal for the production of low cost, large format, high sensitivity and long wavelength FPAs. Finally, we note that the current processes and detector geometry are directly applicable to MW/LW two-color FPAs, and these FPAs are under development.

TYPE II SUPERLATTICE DETECTOR MATERIALS

Although now a relative old concept, the type II superlattice (SL) has been less developed for IR detection than the QWIP. The (Ga,Al)As QWIP benefits from a materials system that is relatively easy to produce with outstanding reproducibility, uniformity and quality. The drawback is its absorption mechanism that leads to a relatively low quantum efficiency and necessitates novel light coupling schemes as the C-QWIP described above. . In contrast, type II SLs that can be produced in the (Al,Ga,In)(As,Sb)-system, can theoretically overcome these shortcomings and even surpass other direct-bandgap materials by reducing Auger recombination by clever SL-band engineering. Unfortunately, this has yet to be demonstrated since many basic materials quality issues remain to be solved.

The prototype type II structure is the InAs/GaSb SL, which can be grown on GaSb substrates. A central issue in the growth technique is the interface engineering. Since both group III and V elements are changed, the interface can in principle be of InSb- or GaAs-type. It is generally accepted that the InSb-version produces better quality material, so a special shutter sequence is usually employed to promote such an interface formation. Introducing InSb also has the benefit of adding strain compensation against

the InAs, thus allowing nearly strain-free structures to be grown on GaSb, within certain limits. In addition, to the designed interface structure, interdiffusion always takes place as seen in detailed cross-sectional scanning tunneling microscopy studies from materials produced in many laboratories – undoubtedly under quite different growth conditions [Ref 16,17]. A detailed microscopic understanding of the structural and electrical (trap) properties of these interfaces is currently not available. It can also be mentioned that the constituent bulk materials show quite high background doping concentrations even when grown under optimized conditions. It has been proposed for example for GaSb that the ubiquitous p-type doping observed is due to a native defect [Ref 18]. To complicate matters further, localized crystalline defects are prone to form in SLs under different growth conditions, interface shutter sequences, and as a consequence of the initial substrate surface quality [Ref 17]

We have grown relatively thin InAs/GaSb SLs for studies of PIN diodes in the MWIR-range. By restricting the initial work to shorter wavelengths the added complication of surface leakage can be avoided. As the wavelength is increased surface passivation quickly becomes essential. The mid-wave structure consisted of a p-doped GaSb bottom-contact, 50 periods of 24+24 Angstrom SL and a 350 A thick, InAs, top, n-contact layer. The less than quarter-micron thick, light-absorbing layer allows collection of nearly all generated electron-hole pairs, which simplifies the detector evaluation. Also, any influence of residual strain, or growth-thickness-dependent defects is expected to be minimal by keeping the overall layer thickness thin. The substrate growth temperature has been optimized based on the line-width of the zero-order peak of the SL. The narrowest peak is at the calculated limit for a structure of this thickness. The growth window is relatively wide as seen in Fig. 8. By careful calibration work and attention to stability details, structures can be grown that are extremely close to the design targets. In this context high-resolution x-ray diffraction
(HRXRD) and simulation tools based on dynamical scattering theory give the most detailed insights. Fig. 9 shows the comparison between data and theory for such an experiment.

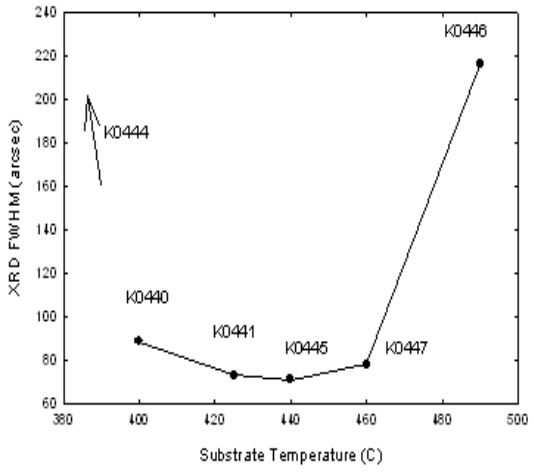

Fig. 8. Full width half-maximum width of the zero-order peak from a 50 period SL grown at different substrate temperatures.

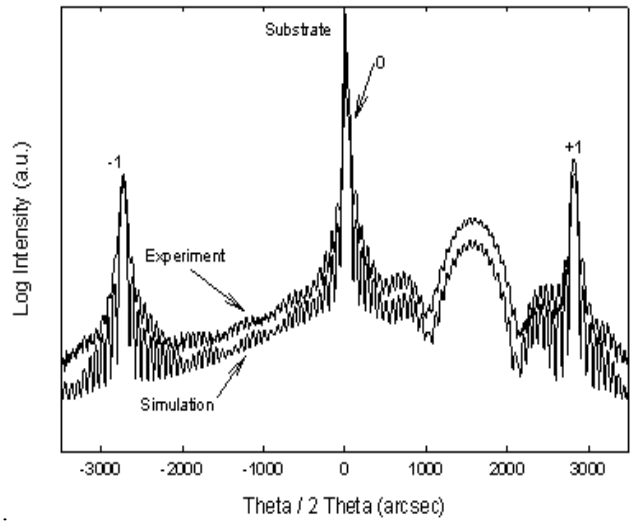

Fig.9 HRXRD experimental data and simulation for a LWIR InGaAs/GaSb superlattice. The fine period oscillations are pendelloesung fringes that demonstrate the flatness and precision of the layer stack. The difference in position between the substrate- and superlattice zero-order peak indicates the residual strain. The higher order peak positions yield the period of the SL. The broad feature at ~ 1500 arcsec is the InAs cap layer. The two curves are offset vertically by a factor of 2 for clarity.

A wafer of this design was fabricated into 320x256 arrays, as well as single-pixel diodes at the III-V foundry at BAE systems at Nashua. In passing can be mentioned that this validates the strategy of using III-V foundries for IR detectors – a fabrication line for MMICs can easily be adapted for production of detector arrays. The structure absorption turn-on is at 4.5 micron. Through a very detailed characterization effort of the test equipment and analysis of the measured data from both the hybridized arrays and the fanned-out single pixels, we were able to reconcile both data sets to arrive at an absorption spectrum from the SL. This also agrees very well with our calculation as seen in Fig. 10. An image from the array is shown in Fig.11 Further details can be found in Ref. 18.

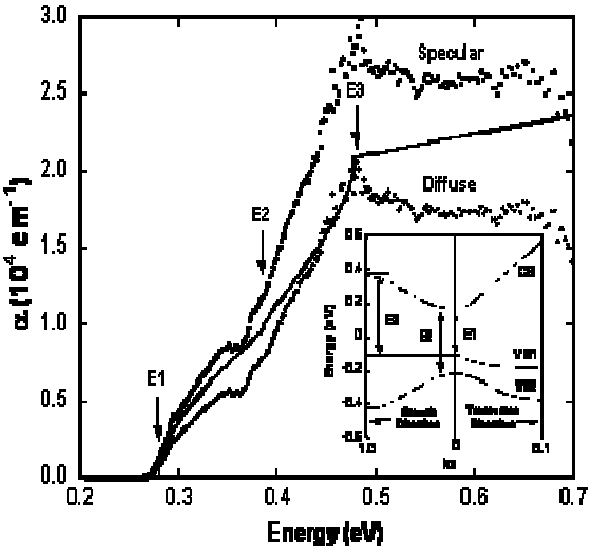

Fig. 10. Experimentally measured (data points) and theoretically calculated (solid line) absorption coefficient for the MWIR type II superlattice material. Experimental results are shown for cases of specular and diffuse transmission at the back surface of the detector. Important transitions (E1, E2, and E3) are labeled on the theoretical curve. The inset shows the results of an 8-band $k \cdot p$ band-structure calculation with transitions E1, E2, and E3 identified.

Fig. 11. 320 x 256 format image taken at 78 K with f/4 dewar optics and 0.75 ms integration time. Most bad pixels are near the perimeter of the array and are probably related to hybridization and mechanical thinning, not poor material quality.

Direct Bandgap III-V Detector Materials

In order to realize the full potential of the type II SL, further improvements are needed in materials synthesis technology. Although good progress has been made, at the moment it is unclear how much additional effort will be needed to eliminate all hurdles in this materials system. It is therefore of interest to also look at other III-V approaches that may not have to rely on SL formation, with the inevitable formation of mixed interfaces and potential localized recombination centers. None of the common III-V semiconductors

have bandgaps that are small enough to absorb at long wavelengths and beyond. With "common" we here refer to Ga, In, Al on the Group III side and As, Sb and P among the Group Vs. These elements and their properties as compound crystals are relatively well known and high quality material can be produced. However, by also considering N and Tl in each group we can reduce the bandgaps significantly and theoretically reach longer wavelengths. We would then obtain a III-V, direct-bandgap, material with the associated high quantum efficiency. Unfortunately, incorporation of either N or Tl, is far from trivial, which presents a different set of materials synthesis problems. We are beginning an effort in studies of dilute-nitrides and have an on-going joint effort with Epitaxial Technologies, LLC on the subject of Tl-incorporation. So far we have demonstrated incorporation of up to 6% Tl in GaAs.

MERCURY CADMIUM TELLURIDE ON SILICON

Current state-of-the-art infrared focal plane arrays are fabricated utilizing HgCdTe material. Large format, low cost, reliable and high performance infrared focal plane arrays (IRFPA) fabricated in Mercury Cadmium Telluride (HgCdTe) would have many applications in the Army's Third Generation IR Imaging Technology. Bulk-grown $Cd_{0.7}Zn_{\sim 0.3}Te$ (CZT) substrates are the natural choice for HgCdTe epitaxy since it is lattice matched to the HgCdTe alloy. However, lack of large area CZT substrate, high production costs, and more importantly, the difference in thermal expansion coefficients between CZT substrates and silicon readout integrated circuits are some of the inherent drawbacks of CZT substrates for 3rd generation applications. Thermal expansion mismatch between the detector substrate and the Read-Out Integrated Circuit (ROIC) is of significant concern for large area IRFPAs that require repeated thermal cycling. Consequently, $Hg_{1-x}Cd_xTe$ detectors fabricated on silicon substrates are an attractive alternative generating considerable interest.

Recent developments in the MBE Chalcogenide buffer layer growth technology on Si substrates has revolutionized HgCdTe research and offered a new dimension to HgCdTe-based IR technology. Like sapphire, Si substrates provide advantages in terms of relatively large area (3 to 6-inch diameter is easily obtained) compared to CZT substrate materials, durability during processing, and reliability to thermal cycling. Innovations in Si-based composite substrates made it possible to fabricate very large-format IR arrays that offer higher resolution, low-cost arrays and more dies per wafer.

MBE MWIR HgCdTe devices have been fabricated on CdTe/Si composite substrates by several organizations (8-14). Using CdTe/Si composite substrate technology, MW FPAs as large as 1K x 1K and 2K x 2K have been demonstrated by Rockwell Scientific Company (RSC) and Raytheon Vision Systems (RVS). However, one draw back of this material system is the presence of a higher dislocation density due to the lattice mismatch between the CdTe/Si and HgCdTe. Despite this high dislocation density, data shows that n-type base layers are of excellent quality with measured electron mobilities comparable to the best reported for MWIR-HgCdTe on bulk CZT substrates. Band gap uniformity with standard deviation of 0.001 for a mean composition of 0.321 across 1.5" radii has been demonstrated (8). R_oA as high as $5x10^7$ Ω-cm^2 with a mean value of $7x10^6$ Ω-cm^2 was measured for cut-off wavelength of 4.8 μm at 77K was reported. Quantum efficiencies up to 63% (with no antireflection coating) for cut-off wavelength of 4.8 μm to 5.4 μm @ 77K are observed. These data confirm that it is possible to obtain high performance MWIR-HgCdTe devices on large area silicon substrates, comparable to performance on layers grown on lattice matched bulk substrates, for the same spectral cut-off.

As detailed above, CdTe/Si composite substrate technology have proven that state-of-the-art large-format short (SWIR) and medium wavelength (MWIR) HgCdTe IRFPA fabrication is possible, as has been demonstrated by RVS and RSC (15). This implies that although a higher defect density exists in the material, it has not proven to be a limitation since device measurements of MW-HgCdTe material grown on either bulk or composite substrates are comparable. However, this statement is no longer accurate when long-wavelength (LWIR) HgCdTe devices are desired. It appears that the smaller band-gap LWIR detectors are much more sensitive to material defects which lead to poor device performance (16) .
The lattice constant of LWIR $Hg_{0.78}Cd_{0.22}Te$ is smaller than that of CdTe with a lattice mismatch between these two materials of ~ 0.26%. In order to match the lattice constant of the composite substrate with LWIR HgCdTe, a ternary or quaternary compound containing CdTe based buffer layers has to be used. There are several choices of eligible binary materials to combine with the base CdTe binary to form appropriate alloys, such as CdSe, ZnTe, BeTe and CdS.

$CdSe_xTe_{1-x}$/Si(211) and LWIR HgCdTe/CST/Si growth

At ARL, $CdSe_xTe_{1-x}$ /Si(211) material grown by Molecular Beam Epitaxy (MBE) has been identified as a potential lattice matched composite substrate for long-wavelength (LWIR) HgCdTe device structures. In this work, a simple growth structure was utilized in order to take advantage of our mature composite substrate CdTe/Si growth technology. For the purposes of this study, a CdSeTe layer was nucleated on top of the CdTe layer using our standard growth process(17). CdSeTe was nucleated at the same temperature as CdTe. Some key points about the growth structure are that both the CdTe layer thickness and the CST layer thickness were typically kept near 5 μm in thickness and that the CdSeTe layer underwent no annealing during growth.

The as-grown layers were evaluated using x-ray double crystal rocking curve (DCRC) measurements and optical microscopy to determine overall layer quality, defect density and surface morphology. Through comparison of CdSeTe layers with 4% Se incorporated, we discovered that the best layers were grown at a temperature between 330 and 360 ^{0}C. Our findings show that within this temperature range no significant difference is observed in terms of surface morphology or x-ray double crystal rocking curve (DCRC) evaluation. Using this optimized growth window, we were able to produce CdSeTe /Si (4% Se) with x-ray full width at half maximum (FWHM) as low as 100 arc-sec, and surface defect densities less than 400 cm^{-2}. Both of these values are better than the typically excepted standards (130 arc-sec and 1000 cm^{-2}, respectively) for high quality composite substrate material. Furthermore, the surface morphology of the CdSeTe/Si is identical to that of baseline CdTe/Si and much better than CdZnTe/Si. These results represent a significant achievement towards our goal of achieving highest quality lattice matched composite substrates for LWIR HgCdTe material growth and device fabrication.

Overall compositional, thickness, and x-ray DCRC uniformity is excellent across a three-inch wafer indicating that CST/Si grown by MBE is indeed a suitable composite substrate material. Overall thickness, composition and x-ray DCRC FWHM was measured at seven discrete points across the sample surface. The average Se composition measured 4.31 % with a standard deviation of only 0.02 %. This value corresponds to a variation in the CdSeTe lattice constant of only 0.0024 Å. X-ray data and thickness also show excellent control over lateral uniformity indicating that CdSeTe/Si grown by MBE has the potential as composite substrate material for large form-factor IRFPAs.

Figure 11: Morphology of CdTe//Si, CdZnTe/Si and CdSeTe/Si layers

Once growth conditions for buffer layer CdSeTe/Si were optimized, the research effort shifted toward growing and characterizing HgCdTe on lattice matched CdSeTe/Si composite substrates. Some of the ARL grown CdSeTe/Si substrates were sent out to RSC for the growth of HgCdTe using RSC MBE systems. HgCdTe grown on these CdSeTe/Si exhibit sharp cut-off wavelengths, smooth surfaces and x-ray FWHM below 100 arc-sec even though the CdSeTe/Si substrate itself measured ~100-120 arc-sec. Typical thickness of HgCdTe was about 10 μm. Measured carrier concentrations at 78K were ~1E15 cm^{-3} and average mobility of approximately 1E5 cm^2/Vsec were obtained. These values are comparable to layers grown on bulk CdZnTe. Measured minority carrier lifetime on a LW HgCdTe/ CdSeTe/Si layer at 78K is in the order of 1 μsec. These lifetime show near theoretical vales at 78K and is comparable to the lifetimes reported for similar cutoff LW-HgCdTe grown on bulk CdZnTe substrates. However, for some grown wafers a slight correction using SRH centers component needed to be added to band-to-band fit for the I-V and RoA vs temperature data.

Electrical performance of devices fabricated on a representative sample of a LW (λ_{co} = 10 μm at 78K) wafer is illustrated in Fig 12. Figure 12a shows a cumulative distribution plot of R_oA values for 18 μm x 18 μm area measured at 78K of 25 photovoltaic devices fabricated on two PEC chips from the same wafer. Diodes are ranked according to increasing R_oA at 78K. A relatively small spread in R_oA can be seen. Mean and median R_oA is 319 Ω-cm^2 and 336 Ω-cm^2 respectively for 18 μm x 18 μm device area size devices. Figure 12b compares the measured current voltage characteristics of these devices. These I-V curves show very little leakage currents with no soft breakdown characteristics in the reverse bias region of I-V curve. This is remarkable in spite of the measured dislocation density on a sister piece of the wafer. Measured dislocation density is in the mid-10^6 cm^{-2} and voids are in the order of 500 per cm^2. Past work has shown that voids on the junction will lead to an increase in the reverse bias junction currents (18,19). This is caused by tunneling associated with dislocations that tend to gather around a void defect. The probability of intercepting a void with a small diode, such as an 18 μm x 18 μm diode, is small for material with a void density of 500 cm^{-2}. With Poisson statistics, the calculated yield for not intercepting a void on a single device is in the order of 99% and this agrees very much with the measured 18 μm x 18 μm devices on this wafer. On the other hand, at 78K measured R_oA is not affected by EPD up to mid-10^6 cm^{-2}. This is consistent with the measured R_oA at 78K as indicated by the Fig 12a.

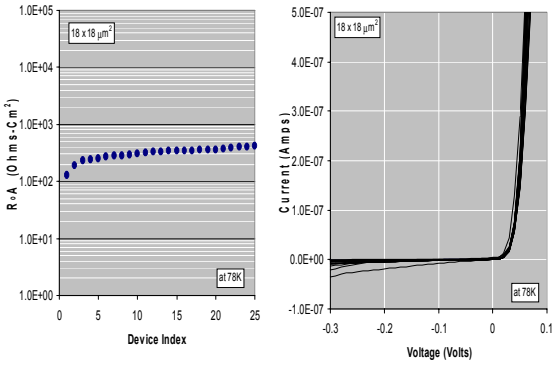

12. a). R_oA cumulative distribution plot at 78K of LW ($\lambda_{co}a$) material from 25 diodes from two PEC chips. Device junction area is 18 µm x 18 µm. b). Measured dark current vs voltage on these devices at 78K.

CONCLUSION

We reported on ARL's material research efforts – if successful - will allow the development of affordable large area high performance Infrared Focal Plane Arrays. All three approaches pursued have their promises, but also have their uncertainties requiring further efforts to resolve these uncertainties. C-QWIPs seem to be the first choice for affordable large area LWIR focal plane arrays. It is still an open question, if C-QWIPs can also be developed for MWIR arrays with sufficient high quantum efficiency. For MCT focal plane arrays, performance in both IR bands is not in question, but if bulk CdZnTe substrates are required, cost considerations will prevent it's use for many applications especially where large area arrays are needed. The use of Silicon based composite substrates would significantly reduce the cost. For SWIR and MWIR focal plane arrays on Si based substrates have been produced with performances equal to arrays grown on CdZnTe substrates. LWIR arrays grown on composite substrates have been produced with good performance characteristics, but reproducibily is still a problem.If theoretical promises could be realized, superlattice detectors would be an ideal choice for both spectral bands since they also promise higher operating temperature, which would further reduce system costs. For dilute Nitrides theory also holds great promises, but it is too early to make any predictions on it's realization.

REFERENCES

1. K. K. Choi, S. V. Bandara, S. D. Gunapala, W. K. Liu, and J. M. Fastenau, "Detection wavelength of InGaAs/AlGaAs quantum wells and superlattices", J. Appl. Phys. 91, 551 (2002).
2. K. K. Choi, K. M. Leung, T. Tamir, and C. Monroy, "Light coupling characteristics of corrugated quantum well infrared photodetectors", J. Quant. Elect. 40, 130 (2004
3. J .Steinshneider, J. Harper, M. Weimer, C.-H Lin, S.S. Pei, D.H. Chow, Phys. Rev. Lett., 85, 4565, 2000

4. J. G. J. Sullivan, A. Ikhlassi, J. Bergman, R.E. DeWames, J.R. Waldrop, C. Grein, M. Flatte, K. Mahlingam, H. Yang, M. Zhong, M. Weimer, J. Vac. Sci. Tech. B23, 1144, 2005
5. J. Shen, J.D. Dow, S.Y. Ren, S.Tehrani, H.Goronkin, J. Appl. Phys. 73, 8313, 1993
6., J. W. Little, S. P. Svensson, W. A. Beck, A. C. Goldberg, S. W. Kennerly, T. Hongsmatip, M. Winn, P. Uppal, J. Appl. Phys. 101, 044514, 2007

7. A. M. Fathimulla et al. (to be published)
8 P.S. Wijewarnasuriya, M. Zandian, D.D. Edwall, W.V. McLevige, C.A. Chen, J.G. Pasko, G. Hildebrandt, A.C. Chen, J.M. Arias, A.I. D'Souza, S. Rujirawat and S. Sivananthan, J. of Electronic Materials, **27**, 546 (1998).
9 . N.K. Dhar, M. Zandian, J.G. Pasko, J.M. Arias and J.H. Dinan, Apl. Phys. Lett. **70**, 1730 (1997).
10. S.M. Johnson, T.J. deLyon, C.A Cockrum, W.J. Hamilton, T. Tung, F.I. Gesswein, B.A. Baumgratz, L.M. Ruzicka, O.K. Wu, J.A. Torh, J. of Electronic Materials, **24**, 467 (1995).
11..J. de Lyon, R.D. Rajavel, J.A. Vigil, J.E. Jenson, O.K. Wu, C.A Cockrum, S.M. Johnson, G.M. Venzor, S.L. Bailey, I. Kasai, W.L. Ahlgren and M.S. Smith, , J. of Electronic Materials, **27**, 550 (1998).
12. G. Brill, S. Velicu, P. Boieriu, Y.P. Chen, N.K. Dhar, T.S. Lee, Y. Selamet and S. Sivananthan; J. Electronic. Mat. **30**, 717(2001).
13. L.A. Almeida, L. Hirsch, M. Martinka, P.R. Boyd, J.H. Dinan, J. Electronic. Mat. 30, 608 (2001).
14. M.F. Vilela, A.A. Buell, M.D. Newton, G.M. Venzor, A.C. Childs, J.M. Peterson, J.J. Franklin, R.E. Bornfreund, W.A. Radford, and S.M. Johnson, , J. of Electronic Materials, **34**, 898 (2005).
15. Nibir K. Dhar and Meimei Z. Tidrow, Proc. SPIE **5564**, 34 (2004)
16. M. Carmody, J.G. Pasko, D. Edwell, R. Bailey, J. Arias, S. Cabelli, J. Bajaj, L.A. Almeida, J.H. Dinan, M. Groenert, A.J. Stoltz, Y. Chen, G. Brill, and N.K. Dhar, , J. of Electronic Materials, **34**, 832 (2005).
17. P. S. Wijewarnasuriya, G. Brill, Y. P. Chen, N. K. Dhar, and S. Velicu, Proc. SPIE **5406**, 323 (2004)
18. M. Johnson, D.R. Rhiger, J.P. Rosbeck, J.M. Peterson, S.M. Taylor and M.E. Boyd; J. Vac. Sci. Technol, **B10**, 1499 (1992).
19 P.S. Wijewarnasuriya, M. Zandian, D.B. Young, J. Waldrop, D.D. Edwall, W.V. McLevige, D. Lee, J. Arias, and A.I. D"Souza, J. Electron. Mater., **28,** 949 (1999)